Three-body constrained bosons in a double-well optical lattice

Suman Mondal,[1] Sebastian Greschner,[2] and Tapan Mishra[1]
[1]*Department of Physics, Indian Institute of Technology, Guwahati-781039, India*
[2]*Department of Quantum Matter Physics, University of Geneva, 1211 Geneva, Switzerland*

(Received 25 January 2019; revised manuscript received 3 April 2019; published 23 July 2019)

We analyze the ground-state properties of three-body constrained bosons in a one-dimensional optical lattice with staggered hoppings analogous to the double-well optical lattice. By considering attractive and repulsive on-site interactions between the bosons, we obtain the phase diagram which exhibits various quantum phases. Due to the double-well geometry and three-body constraint, several gapped phases such as the Mott insulators and dimer–bond-order phases emerge at commensurate densities in the repulsive interaction regime. Attractive interaction leads to the pair formation which leads to the pair–bond-order phase at unit filling, which resembles the valence-bond solid phase of composite bosonic pairs. At incommensurate densities, we see the signatures of the gapless pair superfluid phase.

DOI: 10.1103/PhysRevA.100.013627

I. INTRODUCTION

Ultracold atoms in optical lattices with tunable interactions and lattice parameters have opened up a wide area of research in recent years. The significant progress both in theoretical and experimental fronts has uncovered a wealth of new physics which was impossible to achieve in the conventional solid-state systems. The pathbreaking observation of the superfluid (SF) to Mott insulator (MI) transition [1] following its theoretical prediction [2] in a system of ultracold bosons in an optical lattice has paved the path to simulate complex quantum many-body physics [3]. The exquisite control over the interactions and lattice geometries is the key to achieve such interesting physics. A new frontier of research has evolved with the construction of two-color superlattices, which is an array of double-well potentials [1,4–10]. Recent experiments on systems of ultracold atoms in these double wells have led to various interesting phenomena in condensed-matter physics and also in atom interferometry [9] and quantum information [11]. Particularly in one dimension, these double-well lattices exhibit interesting properties due to the staggered or dimerized hopping amplitudes. The presence of this staggered hopping in this system resembles the inversion symmetric Su-Schrieffer-Heeger (SSH) model for fermions [12] which possess interesting topological features characterized by the Zak phase [13–16]. The model has been generalized to interacting fermions [17,18] and bosons [10,19] and explored in recent experiments [20–24].

On the other hand, the experimental observation of local higher-order interactions in optical lattices has opened up a new direction to simulate quantum phase transitions in the presence of multibody interactions [25]. Several interesting ideas have been proposed to engineer and tune such interactions in optical lattices [26–30]. One such example is the possibility to create a situation where the three-body interaction can become extremely large. Under this circumstance, the bosons experience three-body hardcore constraint [29], which prohibits more than two atoms from occupying a single lattice site. This condition facilitates the exploration of the physics of the attractive Bose-Hubbard model, which otherwise leads to the collapse of atoms onto a single site. Many novel scenarios have been investigated recently by considering three-body constrained bosons in optical lattices [29,31–39]. The physics which is manifested by the two-body interaction along with the large three-body repulsion is one of the simplest problems to understand, although it has interesting physical implications. In such a scenario, the system exhibits the usual SF-MI phase transition for repulsive on-site interaction and for attractive interactions there exists a superfluid to pair-superfluid (PSF) phase transition [31].

In this paper, we consider a system of three-body constrained bosons in a double-well optical superlattice in one dimension, which resembles the SSH type model, as shown in Fig. 1. The presence of double-well potentials creates a situation with staggered hopping amplitudes. This superlattice geometry can be created by superimposing two lattices, with one lattice having double the period of the other.

The physics of ultracold bosons in a double-well optical lattice can be explained by a modified Bose-Hubbard model with staggered hopping amplitudes (bosonic SSH model), which is given as

$$\mathcal{H} = -t_1 \sum_{i\in \text{odd}} (a_i^\dagger a_{i+1} + \text{H.c.}) - t_2 \sum_{i\in \text{even}} (a_i^\dagger a_{i+1} + \text{H.c.}) + \frac{U}{2}\sum_i n_i(n_i-1), \quad (1)$$

where $a_i^\dagger$ and a_i are the creation and annihilation operators for bosons at site i, and $n_i = a_i^\dagger a_i$ is the number operator at site i. t_1 and t_2 are the tunneling rates from odd and even sites, respectively (compare Fig. 1). The on-site contact interactions are characterized by the term U. The bosons in the lattice enjoy three-body constraint, i.e., $(a_i^\dagger)^3 = 0$.

At half filling, the single-particle spectrum of the model given by Eq. (1) exhibits a gap for any imbalance in hopping

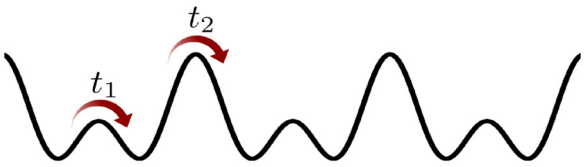

FIG. 1. One-dimensional double-well optical superlattice with staggered hoppings $t_1 > t_2$.

between the unit cells, $t_1 \neq t_2$ [12]. Hence, the ground state is a dimer phase or bond-order (BO) phase for spin-polarized fermions or bosons with very large on-site interactions (hard-core bosons). The presence of three-body constraint may lead to interesting phenomena in such a dimerized lattice, which will be the topic of this paper. In particular, we study the interplay between the pairing of particles and dimerization which gives rise to the emergence of a pair–bond-ordered phases with a sharp crossover to the bond-ordered phase. We assume $t_1 = 1$ (unless stated otherwise), which makes other physical quantities dimensionless. The ground-state properties of this system are analyzed using the density matrix renormalization group (DMRG) method. We consider system sizes up to 160 sites and retaining up to 800 density matrix eigenstates.

The rest of the paper is arranged as follows. In Sec. II, we discuss the limiting cases, focusing on hardcore bosons in the optical lattice made up of a series of double wells and the physics in the limit of isolated double wells. In Sec. III, we present the general phase diagram with different values of two-body on-site interactions. In Sec. IV, we give a brief summary of the work.

II. LIMITING CASES

We begin our discussion with a short summary of the properties of two analytically solvable limits of model (1). These analysis will help in understanding the physics of the system discussed in the paper.

A. $U = \infty$ limit

In the limit of large interactions $U \to \infty$, the bosons are hardcore in nature and, in this limit, model (1), after a Jordan-Wigner transformation to free fermions, can be considered as the topological SSH model as mentioned before. Due to the staggered hopping amplitudes, the SSH model at half filling dimerizes naturally due to the Peierls instability and one gets a dimerized phase of bosons. In this phase, a single boson lives in one of the unit cells composed of two lattice sites in the double well with larger hopping strength. Doping away from half filling breaks this dimer ordering and a critical SF phase appears. This gapped phase is called the BO phase. Note that this BO phase, stabilized due to a spin-Peierls-like mechanism [40], does not exhibit spontaneous symmetry breaking and the BO order is induced due to the explicitly broken translational symmetry of the model. In the literature, this phase is, hence, also called the fractional Mott-insulator phase or similar phase [19]. The phase diagram of such system is shown in Fig. 2 as a function of t_2 and the filling. The gapped phases are characterized by the finite single-particle gaps, which are

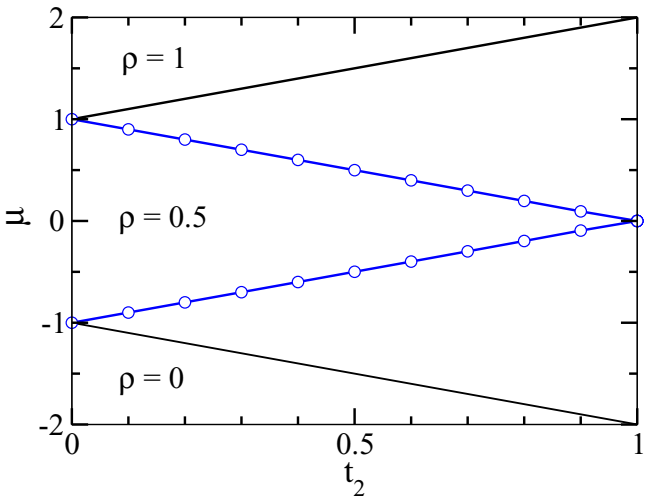

FIG. 2. Phase diagram of hardcore bosons in the $\mu - t_2$ plane with $t_1 = 1.0$. The points correspond to extrapolated DMRG data with $L = 300$, which accurately lie on top of the analytical curves (solid lines). The region included by the blue circles is the gapped bond-ordered (BO) phase at half filling. The gap opens up for any finite dimerization t_2/t_1. The black curves represent the empty and full states.

defined as

$$E_G = \mu^+ - \mu^-, \tag{2}$$

where μ^+ and μ^- are the chemical potentials. As can be seen from the phase diagram, any finite hopping imbalance leads to the gapped phase which is a bond-ordered (BO) phase and this phenomenon is also evident from the single-particle spectrum.

B. Isolated double wells

It is also instructive to discuss the model for the case of trivially disconnected double wells, corresponding to the case $t_2 = 0$. From this limit, one can conveniently explain the finite hopping case, which is the topic of interest of the paper. In this limit, the model Hamiltonian can be readily diagonalized for a fixed particle number: In the $n = 1$ ($n = 3$) sector, two eigenenergies $\pm t_1$ ($U \pm 2t_1$) are found. For $n = 2$, the eigenvalues are given by U and $\frac{1}{2}(U \pm \sqrt{16t_1^2 + U^2})$. With these eigenvalues in a grand-canonical ensemble, three gapped phases at fillings $\rho = 0.5$, 1, and 1.5 can be observed, as shown in Fig. 3, in the strong dimerization limit. In this limit, the gap at unit filling is given by $E_G = -3t_1 + \sqrt{16t_1^2 + U^2}$.

The ground state in the $n = 1$ sector is given by $|\psi_1\rangle = \psi_{20}|2, 0\rangle + \psi_{11}|1, 1\rangle + \psi_{02}|0, 2\rangle$. Here, $|n_1, n_2\rangle$ denotes a Fock-state basis of the isolated double well and $\psi_{02} = \psi_{20} = 2/\sqrt{16t_1^2 + 2U\varepsilon}$, $\psi_{11} = 2\varepsilon/\sqrt{16t_1^2 + 2U\varepsilon}$, where $\varepsilon = U/2 + \sqrt{4t_1^2 + U^2/4}$. For $U \to \infty$, this results in a MI-like state $\sim |11\rangle$ and a dimer of pairs $|20\rangle + |02\rangle$ [pair–bond-ordered (PBO) phase] for strong attractive interactions with a smooth crossover between both regimes. Indeed, the decoupled double-well ground state for $U = 0$ resembles a superposition of the MI and PBO states. The features of this interesting many-body state for finite hopping $t_1, t_2 \neq 0$ will be studied in Sec. III.

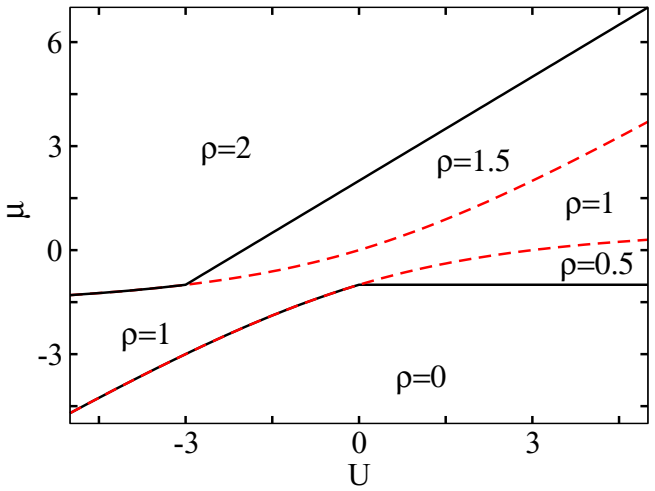

FIG. 3. Phase diagram of isolated double wells showing three gapped phases at $\rho = 0.5$, 1, and 1.5.

A finite small hopping $0 < t_2 \ll 1$ will couple the double wells and allow for a melting of the gapped phases due to the energy gain by delocalization of the excitations, and will stabilize superfluids separating the gapped phases. This process may be understood as well from a effective model of coupled dimer states such as recently discussed in Refs. [41,42].

III. GENERAL PHASE DIAGRAM

In this section, we discuss the most general model with finite on-site interaction and finite hoppings. To start with, we consider the case of vanishing interaction and then we switch on interaction to see the effect of dimerized hopping on the physics of the system. As our main finding, we discuss the emergence and crossover between the various gapped phases such as bond-order, pair–bond-order, and Mott-insulator phases. We show how these phases may be characterized by their different measurables such as the dimerization and their characteristic parity order.

A. Vanishing two-body interaction ($U = 0$)

In the limit of vanishing interactions for a softcore boson without the three-body hardcore constraint, one expects an SF phase even for very strong hopping imbalance. In the presence of interaction, the physics of the system is governed by the competition between the hopping amplitudes and the on-site interactions, which leads to the nontrivial gapped phases at intermediate half-integer filling apart from the gapped MI phases [19] as a function of interaction U. A similar feature is also present in the case of a usual two-color superlattice potential where the SF phase becomes gapped MI phases at half integer and integer fillings for strong interactions [43]. The situation, however, is different in the case of three-body constrained bosons where a maximum of two bosons can occupy a single lattice site. Due to the effect of the double-well superlattice, the motion of particles is restricted to one unit cell. Interestingly, in such a scenario, two different gapped phases arise at $\rho = 1$ and $\rho = 1.5$ after some critical values of t_2. The gap in the system can be seen as the finite plateaus

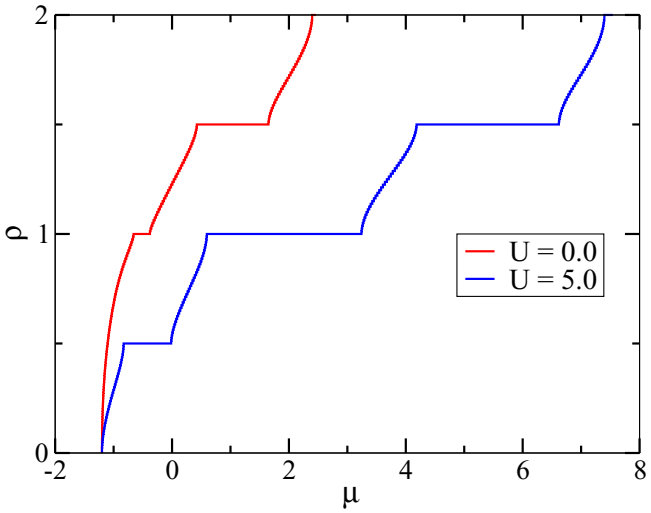

FIG. 4. The behavior of ρ with respect to μ for $U = 0$ (left red curve) and $U = 5$ (right blue curve) for $t_2 = 0.2$. Plateaus indicate the gapped phases.

in the ρ vs μ diagram, as shown in Fig. 4. The phase diagram corresponding to this scenario is depicted in Fig. 5 where the gapped phases at $\rho = 1$ and $\rho = 1.5$ appear at $t_2 \sim 0.4$ and $t_2 \sim 0.9$, respectively. The gapped BO regions for $\rho = 1$ and $\rho = 1.5$ are bounded by red circles and blue squares, respectively. The black lines correspond to the empty and full states. The remaining part of the phase diagram is the SF phase.

B. Finite U and $t_2 = 0.2$ case

As the system is already in the gapped BO phase for $U = 0$ at commensurate densities except at $\rho = 0.5$, it is interesting to see the effect of interactions on the ground state of the system. The phase diagram for this case is shown in Fig. 6. As we move away from the $U = 0$ limit along the positive

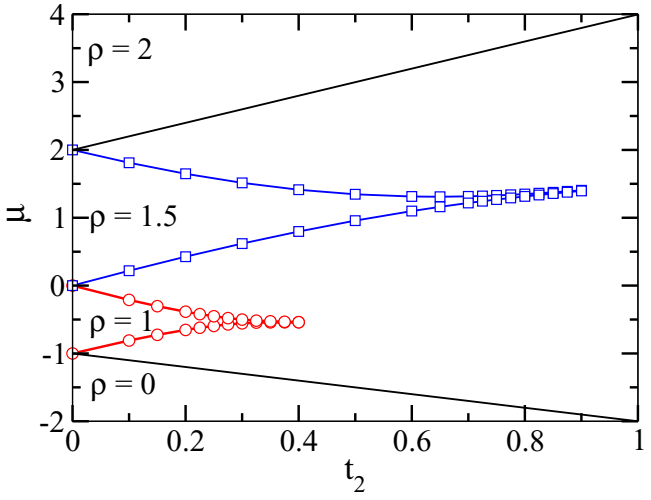

FIG. 5. The phase diagram for three-body constrained bosons as a function of t_2 for $U = 0$ obtained from polynomial extrapolation of the gap. The BO phase at $\rho = 1$ and $\rho = 1.5$ appears at $t_2 \sim 0.4$ and $t_2 \sim 0.9$, respectively.

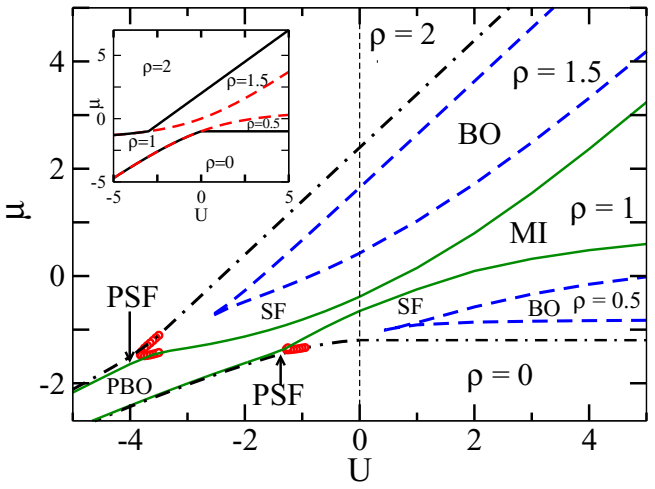

FIG. 6. Phase diagrams for $t_2 = 0.2$. The regions bounded by the green curves are the gapped phases at $\rho = 1$(middle) which consists of the MI (PBO) phases in the strong repulsive (attractive) regimes. The regions bounded by the blue dashed curves are the gapped BO phases at $\rho = 0.5$ (upper) and $\rho = 1.5$ (lower). On the attractive side, the PSF is separated from the SF phase by the red circles. Inset: The phase diagram in the limit of isolated double wells for comparison.

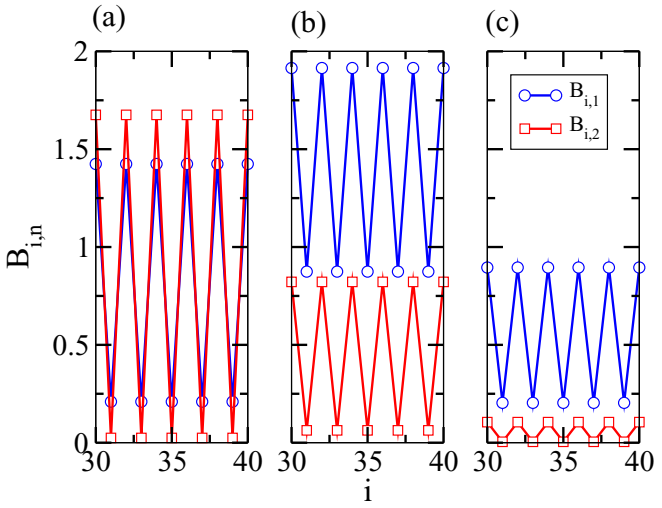

FIG. 7. Bond operator $B_{i,n}$ is shown for the BO (blue circles) and PBO (red squares) phases for $\rho = 1$ and $t_2 = 0.2$. (a) $B_{i,n}$ for $U = -4$. (b) $B_{i,n}$ for $U = 0$. (c) $B_{i,n}$ for $U = 8$.

U axis, the gapped phases grow as can be seen from the enlargement of the plateaus in the ρ vs μ plot for $U = 5$ shown in Fig. 4. The gapped phases at $\rho = 0.5$ and $\rho = 1.5$ are depicted by the region bounded by the blue dashed curves and the one at $\rho = 1$ is bounded by the green solid curve in the phase diagram of Fig. 6. At $\rho = 0.5$, the gap appears after a critical point $U \gtrsim 0.4$ leading to the BO phase. As anticipated in the discussion of the decoupled double-well case, the excitation gap at $\rho = 1$ remains finite for all U, even for a small $t_2 > 0$ leading to a smooth crossover from the pair–bond-ordered (PBO) phase to the MI phase through the BO phase, where every site is occupied by one atom due to large on-site repulsion. The strong on-site repulsion disfavors the dimerization and prohibits two particles from occupying a single site. For $\rho = 1.5$, the system remains in the BO phase, which becomes wider as a function of U. This BO phase is similar to the one for the hardcore bosons at $\rho = 0.5$, as discussed before. The boundaries for the gapped phases are obtained by computing the chemical potentials μ^+ and μ^- and extrapolating them to thermodynamic limit using system sizes of $L = 20,\ 40$, and 80.

The signatures of the BO and PBO phases can be seen by plotting the bond operator,

$$B_{i,n} = \langle (a_i^\dagger)^n (a_{i+1})^n + \text{H.c.} \rangle, \tag{3}$$

for different bonds. Here, the exponent $n = 1$ and $n = 2$ for the BO and the PBO phases, respectively. In Fig. 7, we plot $B_{i,n}$ for unit filling, which show finite oscillations in the BO and PBO phases. The calculations are done by taking 80 sites and, in the figure, we show only the central part of the system. Figures 7(a)–7(c) shows the values of $B_{i,n}$ for $U = -4$, 0, and 8, respectively. The strong oscillation of the PBO operator compared to the BO operator for $U = -4$ shows that the system is dominantly in the PBO phase. Also it can be seen that for $U = 8$, the oscillation of $B_{i,n}$ has decreased drastically due to the MI phase. Similarly, in Figs. 8(a) and 8(b), we plot the value of $B_{i,n}$ for $\rho = 0.5$ and $\rho = 1.5$, respectively, for the repulsive values of U where the system is in the BO phase.

Further, we obtain the signature of the BO phases by computing the bond-bond correlation function and the related structure factor, which is given as

$$S_{\text{BO}}(k) = \frac{1}{L^2} \sum_{i,j} e^{ikr} \langle B_i B_j \rangle, \tag{4}$$

where $r = |i - j|$ is the distance. In the BO phase, the quantity B_i oscillates in alternate bonds and the structure factor exhibits a finite peak at the zone boundaries. It is to be noted that the BO phases which appear in the phase diagram are not the true BO phase as the lattice translational symmetry is not spontaneously broken. However, the signature is similar to

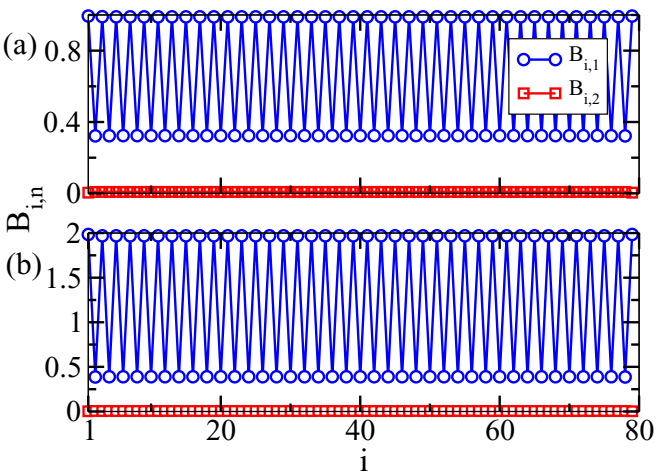

FIG. 8. Bond operator $B_{i,n}$ is shown for the BO (blue circles) and PBO (red squares) phases for $t_2 = 0.2$. (a) $B_{i,n}$ for $U = 4$ and $\rho = 0.5$. (b) $B_{i,n}$ for $U = 2$ and $\rho = 1.5$.

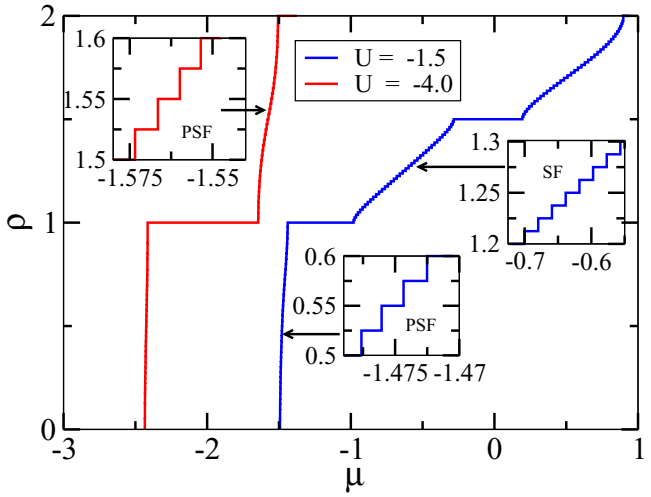

FIG. 9. Behavior of ρ with respect to μ for $U = -4.0$ (left red curve) and $U = -1.5$ (right blue curve) at $t_2 = 0.2$. Insets: The enlarged regions of the SF and PSF phases where the density jumps in steps of one and two particles, respectively.

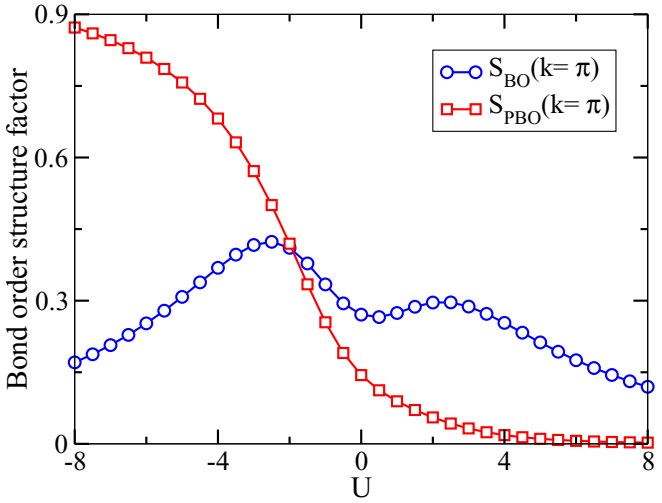

FIG. 10. The extrapolated values of the bond-order structure factor for a single particle (blue circles) and pairs (red squares) for different values of U at $\rho = 1$ (see text for details). Here, $t_2 = 0.2$.

the BO phase, whose qualitative feature can be seen from the bond-order structure factor.

The situation becomes interesting in the attractive regime. Because of the three-body constraint, the system is stable against collapse and, due to the attractive interaction, the particles start to form pairs. While there is no gapped phase at $\rho = 0.5$ in this side of the phase diagram, the gap at $\rho = 1.5$ remains finite up to some finite values of U and then closes after a critical point of $U = -2.6$. The closing up of the gap is due to the competition between the hopping and attractive interaction which tries to break the dimerization and the system becomes a superfluid, as shown in Fig. 6. However, for $\rho = 1$, the gap survives for very large values of U extending up to infinity. These features can be seen from the plateaus in the $\rho - \mu$ plot as shown in Fig. 9 for two different values of $U = -1.5$ and $U = -4.0$. For $U = -1.5$, the gaps appear at $\rho = 1$ as well as at $\rho = 1.5$, whereas for $U = -4$, only the gap at $\rho = 1$ exists. For sufficiently strong attractive interactions, the particles tend to form pairs and, at unit filling, it becomes a half-filled system of bosonic pairs. It is to be noted that these pairs behave like hardcore bosons due to the three-body constraint. In such a scenario, the ground state is similar to the dimerization of the hardcore bosons, as discussed in the section for the $U = \infty$ case. The gapped phase for large attractive U is the BO phase of pairs which can be called the PBO phase. However, in the weak interaction regime, pair formation is not favored due to the competition between the interaction and kinetic energy. Therefore, the BO phase which appears at $U = 0$ survives up to a finite value of attractive U and then there exists a smooth crossover to the PBO phase as the value of U increases.

The characteristic feature of the PBO phase is seen from the PBO structure factor $S_{\mathrm{PBO}}(k)$, which is similar to the BO structure factor as defined in Eq. (4), with $a^\dagger(a)$ replaced by $a^{\dagger 2}(a^2)$, which is shown in Fig. 10. It can be seen that the value of $S_{\mathrm{PBO}}(k = \pi)$ increases smoothly as the value of U becomes more and more attractive. At the same time, the BO structure factor $S_{\mathrm{BO}}(k = \pi)$ decreases smoothly after increasing up to a particular value of attractive interaction, $U \sim -2.5$. Note that the finite value of $S_{\mathrm{PBO}}(k = \pi)$ for repulsive U and small attractive U is due to the finite probability of second-order hopping processes in the BO phase. We would like to stress that since the BO phases are the manifestation of the double-well geometry of the lattice, the BO structure factor remains finite even in the the MI and PBO phase and even in the thermodynamic limit. It can be seen from Fig. 10 that on the repulsive interaction side, the value of $S_{\mathrm{BO}}(\pi)$ smoothly decreases after a particular value of U. This signals the crossover to the MI phase. The onset of the MI phase can be understood as in the case of large interaction U, where the system prefers to accommodate one particle in each site which is also true in the homogeneous lattice systems. This can be seen from the decreasing trend of the curve shown in Fig. 10.

We may further characterize the position of the phase crossover by local maximum of the fidelity susceptibility [44], which is defined as

$$\chi_{\mathrm{FS}}(U) = \lim_{U - U' \to 0} \frac{-2 \ln |\langle \Psi_0(U) | \Psi_0(U') \rangle|}{(U - U')^2}, \qquad (5)$$

with the ground-state wave function $|\Psi_0\rangle$. While the phase transitions are often characterized by a peak diverging with the system size L, here we observe a stable maximum as a function of several system sizes, as shown in Fig. 11.

The gapped BO phase which continues from the repulsive side for $\rho = 1.5$ closes at a critical value $U \sim -2.6$. It is interesting to note that as the interaction becomes more and more attractive, the pair formation occurs and a PSF phase is stabilized for all densities around $\rho = 1.0$ [31,34]. The PSF and SF phases are separated by the red circles as depicted in the phase diagram of Fig. 6. The signature of the PSF phase can be obtained from the $\rho - \mu$ plot, where the density jumps in steps of two particles at a time to minimize the energy. This is clearly visible in the insets of Fig. 9, where the densities for two different values of U are plotted. For $U = -1.5$, the system is in a PSF phase in the region below the $\rho = 1$

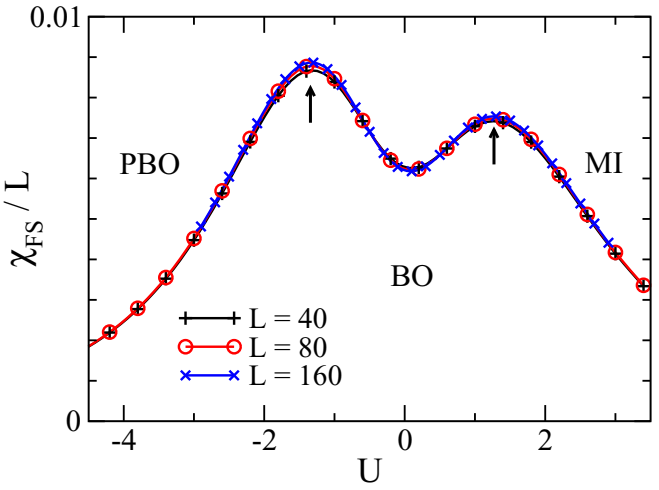

FIG. 11. Fidelity susceptibility χ_{FS} as function of the interaction strength U ($\rho = 1, t_2 = 0.2$) for $L = 40$, 80, and 160.

gapped phase and the rest of the region is in the SF phase for incommensurate densities.

However, for $U = -4$, the system is in the PSF phase for all values of density except $\rho = 1$. Apart from the $\rho - \mu$ curve, we compute the single-particle and pair correlation functions and the corresponding momentum distribution to confirm the existence of the PSF phase. Figure 12 shows the behavior of $\Gamma(i, j) = \langle a_i^\dagger a_j \rangle$ (black circles) and $\Gamma_{\text{pair}}(i, j) = \langle (a_i^\dagger)^2 (a_j)^2 \rangle$ (red squares) with respect to the distance $|i - j|$ for $U = -4$ and $\rho = 1.5$. It can be clearly seen that the single-particle correlation function decays faster, whereas the pair correlation function behaves like a power law in the logarithmic scale, which indicates the presence of the PSF phase.

We also compute the momentum distribution function as

$$N(k) = \frac{1}{L} \sum_{i,j} e^{ikr} \Gamma(i, j) \tag{6}$$

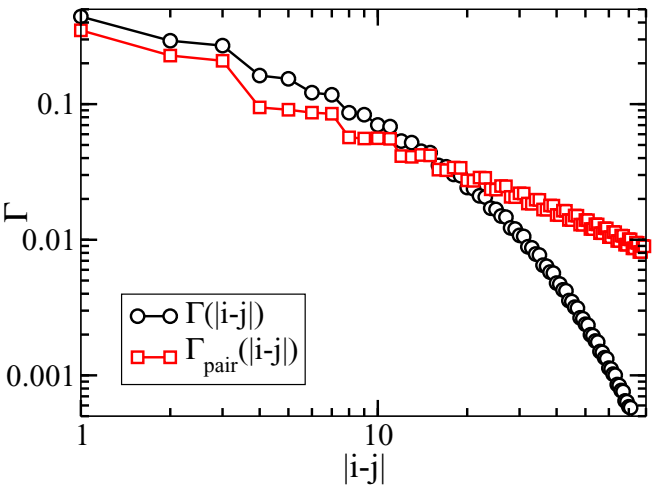

FIG. 12. Single-particle correlation function $\Gamma(|i - j|)$ (black circles) and pair correlation functions $\Gamma_{\text{pair}}(|i - j|)$ for $t_2 = 0.2$ are plotted for $U = -4.0$ at $\rho = 1.5$ for a system of length $L = 160$ (see text for details).

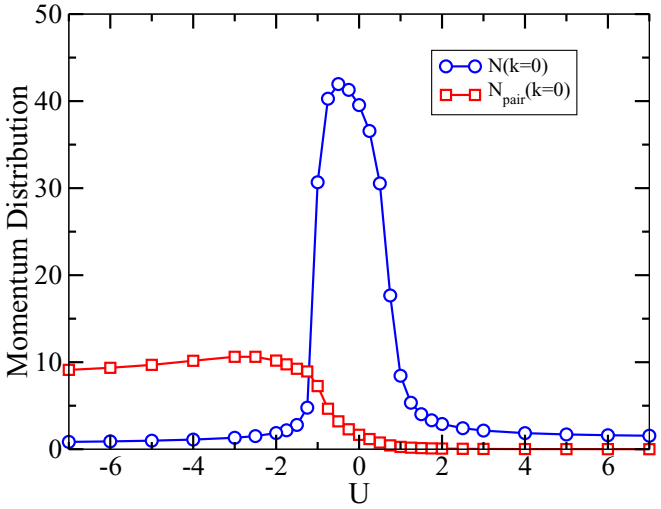

FIG. 13. The peak heights of $N(k = 0)$ (blue circles) and $N_{\text{pair}}(k = 0)$ (red squares) at $\rho = 0.5$ using $L = 160$ for $t_2 = 0.2$ show the transition from PSF to SF, and then to BO phases, as discussed in the text.

to complement the SF phases. Where $\Gamma(i, j) = \langle a_i^\dagger a_j \rangle$ ($\langle a_i^{\dagger 2} a_j^2 \rangle$) is the single-particle (pair correlation) function. The peak heights of the momentum distribution function $N(k = 0)$ for a single particle and pairs are plotted against U in Fig. 13 for a cut through the phase diagram of Fig. 6 which corresponds to $\rho = 0.5$. This shows that for a large attractive interaction, $N_{\text{pair}}(k = 0)$ is dominant, indicating the PSF phase. As the value of U becomes less attractive, the value of $N_{\text{pair}}(k = 0)$ decreases and $N(k = 0)$ increases, showing the signatures of the SF phase. The SF phase continues until the critical point for the SF-BO transition on the repulsive side, where both momentum distribution functions are extremely small. The SF-BO transitions are a Berezinskii-Kosterlitz-Thouless (BKT)-type transition, which can be seen from the smooth opening up of the gap in Fig. 6. The transition points can be accurately obtained by performing a finite-size scaling of the single-particle momentum distribution function, which varies as $N(k = 0) \propto L^{1-\frac{1}{2K}}$ [45], where $K = 2$ is the Luttinger parameter. In Fig. 14, we plot $N(k = 0)L^{-3/4}$ for different lengths ($L = 80$, 120, 160) and all the curves intersect at the critical point $U \sim 0.44$.

At this point, we analyze the system without the three-body hardcore constraint to see the effect of finite three-body interactions $(W/6) \sum_i n_i(n_i - 1)(n_i - 2)$ in the presence of the double-well potentials. As already mentioned before, for softcore bosons and vanishing two-body interaction, i.e., $U = 0$, the system is a gapless superfluid for any value of hopping dimerization, which is in contrast to the case of three-body constrained bosons. To see the effect of finite W, we analyze the ρ vs μ plot for different values of $W = 0$, 5, and 10 considering $L = 40$ with small on-site interaction $U = 1$, which is shown in Fig. 15. Here we can see that for $W = 0$, the system is in the SF phase for integer and half-integer densities, except at half filling where there exists a small plateau. This is consistent with the result obtained in Ref. [46]. However, as the value of W increases, the plateaus at other integer

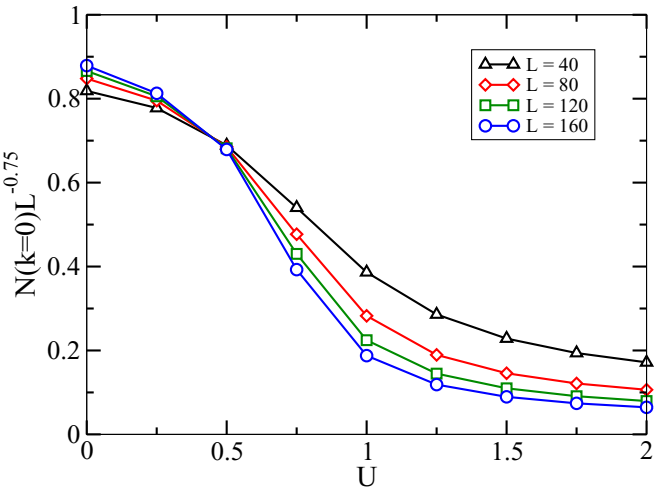

FIG. 14. Finite-size scaling of $N(k=0)$ for $t_2 = 0.2$ shows that the curves for different lengths ($L = 40$, 80, 120, 160) intersect at the critical point $U \sim 0.44$ for the SF-MI transition at $\rho = 0.5$.

and half-integer densities appear, indicating various gapped phases. The plateau lengths increase in size with an increase in W. Therefore, we would like to highlight that although the three-body hardcore constraint is essential to stabilize the gapped phases on the attractive U side, it is not that crucial for the repulsive U case.

C. Finite U and $t_2 = 0.6$ case

After analyzing the phase diagram for the $t_2 = 0.2$ case where the effect of staggered hopping is large, we repeat the calculation for another cut through the phase diagram of Fig. 5 at $t_2 = 0.6$. The motivation to consider $t_2 = 0.6$ lies in the fact that there is no gap at $\rho = 1$ for $U = 0$, as depicted in Fig. 5, and it will be interesting to see how the system evolves by

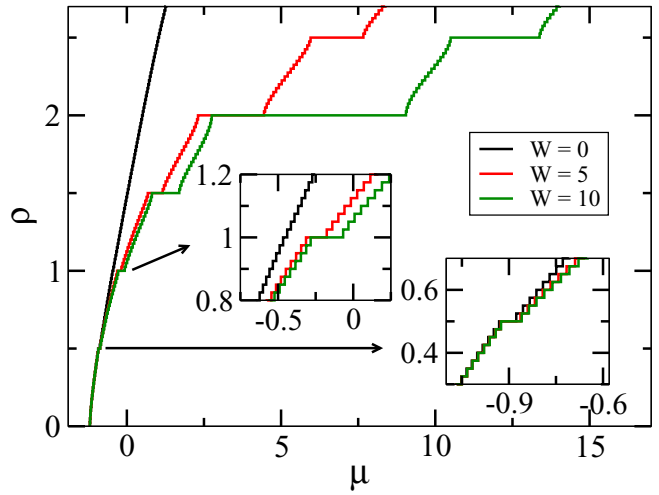

FIG. 15. Behavior of ρ with respect to μ for $U = 1$, $t_2 = 0.2$, and $W = 0$ (black curve), $W = 5$ (red curve), and $W = 10$ (green curve) for the case of softcore bosons. Here the maximum number of particles per site is taken to be 5. Inset: The zoomed-in view of the $\rho = 1$ and 0.5 regions.

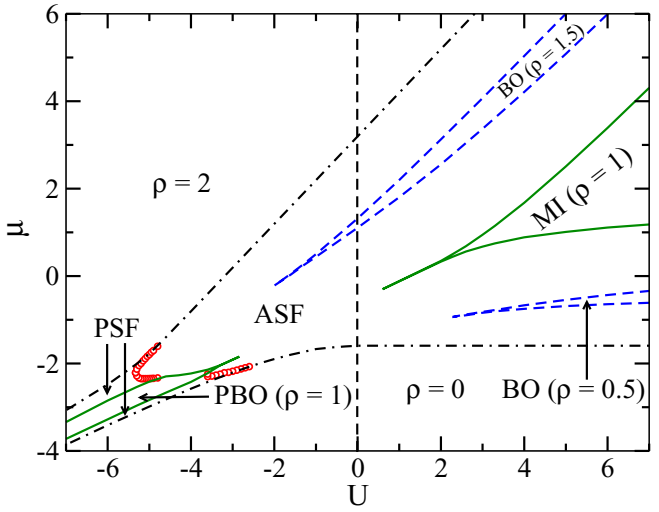

FIG. 16. Phase diagrams for $t_2 = 0.6$. The regions bounded by the continuous green curves are the gapped phases at $\rho = 1$ and the regions bounded by the blue dashed curves are the gapped bond-order phases at $\rho = 0.5$ (upper) and 1.5 (lower). On the negative U side, the PSF is separated from the SF phase by the red circles. The black dot-dashed lines represent the empty and full states.

moving away from this limit. A similar analysis along the line of the $t_2 = 0.2$ case leads to the phase diagram as shown in Fig. 16. It can be seen that the overall picture of the phase diagram is similar to that of $t_2 = 0.2$ for $\rho = 0.5$ and $\rho = 1.5$. However, it is interesting to note that there are clear phase transitions from the SF phase to the MI phase on the repulsive side of U and to a PBO phase on the attractive side of U. These signatures can be clearly seen from various order parameters plotted in Fig. 17. It can be seen that the PBO structure factor, gap, and parity order (see Sec. III D for detail) remain finite in the gapped MI and PBO phases, whereas they vanish in the SF phase.

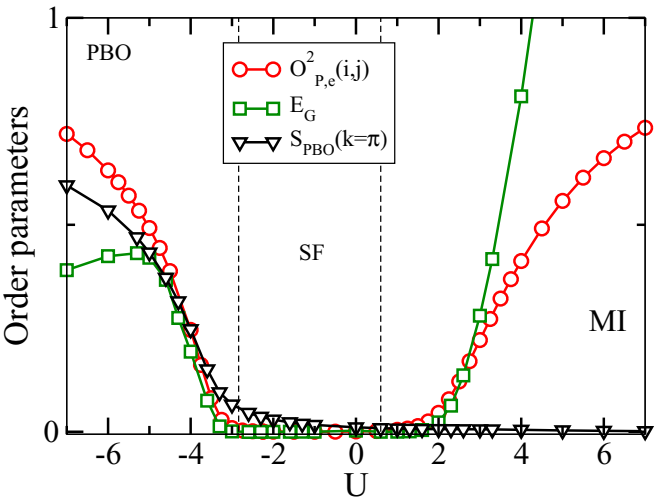

FIG. 17. Order parameters depicting different phases for $t_2 = 0.6$. The red circles, green squares, and black down-triangles show the values of $O^2_{P,e}(i,j)$, $E_G(L)$, and $S_{\mathrm{PBO}}(k=\pi)$, respectively, for different values of U.

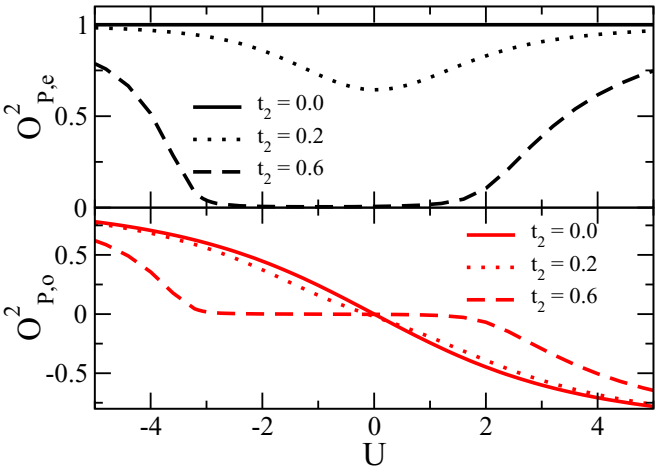

FIG. 18. Parity order $O^2_P(i, j)$ for odd and even distances $|i - j| \gg 1$ are plotted for different values of t_2 with respect to U. $t_2 = 0$ lines correspond to the analytical results, as discussed in the main text; $t_2 = 0.2$ and $t_2 = 0.6$ curves depict the data obtained for $L = 160$ sites.

D. Parity order

Another physical quantity of interest which can be directly accessed in the state-of-the art experiment [47,48] is the parity order parameter, which is defined as

$$O^2_P(i, j) = \left\langle e^{i \sum_{i<k<j} \pi n_k} \right\rangle. \tag{7}$$

To complement our findings, we compute $O^2_P(i, j)$, which is finite in the MI phase due to particle-hole excitations. For small $t_2 \to 0$, we may understand the emergence of parity order from the properties of isolated double wells, as discussed in Sec. II B. For a ground state at $\rho = 1$ given by a product of $|\psi_1\rangle$, one easily estimates the parity order to be exactly $O_{P,e} = 1$ on even distances $|i - j|$. For odd distances, however, one observes an interesting dependence of the parity order on the interaction strength, $O_{P,o} = -\frac{U}{\sqrt{16t_1^2+U^2}}$. We plot the odd and even distance parity orders as $O_{P,e}$ and $O_{P,o}$, respectively, with respect to U for different values of t_2 in Fig. 18. The black and red curves correspond to $O_{P,e}$ and $O_{P,o}$, respectively. The solid lines correspond to the limit of isolated double wells, i.e., for $t_2 = 0$. The dotted lines are the $t_2 = 0.2$ and the dashed curves are for $t_2 = 0.6$. It is very clear from this figure that the odd and even distance parities show two different behaviors and the parity order is finite in the MI, BO, and PBO phases, whereas it is zero in the SF phase. Analogously, one also finds, for the gapped phases at half filling, a finite oscillating parity order which is 0 for even and ± 1 for odd distances. The parity order parameter also vanishes in the SF phase. This can be seen from Fig. 19, where $O^2_{P,e}$ is plotted as a function of U for different fillings.

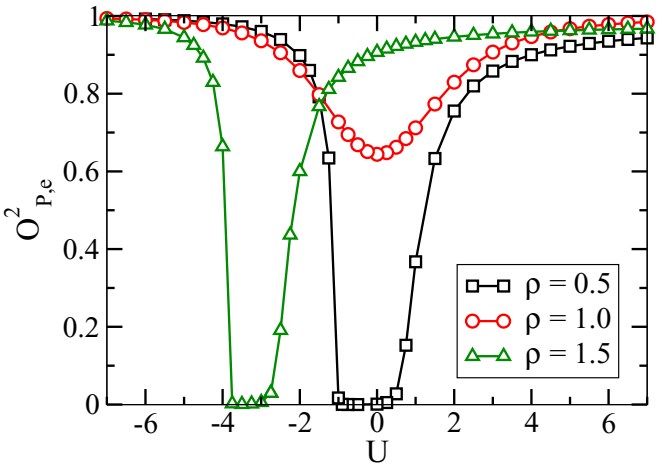

FIG. 19. $O^2_{P,e}$ at $\rho = 0.5$, 1.0, and 1.5 for $t_2 = 0.2$ is plotted for different values of U.

IV. CONCLUSIONS

We investigated the ground-state phase diagram of a system of three-body constrained bosons in a double-well optical lattice. By analyzing the competition between the dimerized hopping and on-site interactions, we obtained the complete phase diagram both in the regime of attractive as well as repulsive interactions. The phase diagram exhibits various gapped phases such as the BO and MI phases at commensurate densities. At unit filling and small hopping ratios, the system exhibits a BO phase of pairs in the attractive interaction regime, which we call the PBO phase, and there exists a smooth crossover from MI-BO (BO-PBO) on the repulsive (attractive) side of the phase diagram. For large values of the hopping ratios, the gapped phases melt for small values of interactions and there exists an intermediate SF phase. The appropriate finite-size scaling shows that the superfluid to gapped phase transitions are of the BKT type. The findings presented in this work address an interesting problem which involves the physics of strongly correlated bosons in a double-well optical lattice both in the attractive and repulsive regimes. As the double-well optical lattices have already been created and manipulated using cold atoms, it will be possible to observe these phases in the experiments.

As mentioned before, this kind of double-well optical lattice resembles the topological SSH model discussed in the context of solitons in polyacetylene, which possess two types of dimerizations depending on the hopping ratios. The SSH model exhibits a topological phase transition from a trivial to nontrivial phase through a gapless point. The nontrivial phase is characterized by zero-energy edge modes. The topological aspects of this model have been analyzed recently in various contexts [18,19,49–51]. One interesting phenomenon which signals these topological phase transitions is the Thouless charge pumping mechanism [21,23,52,53]. In the present scenario, the PBO phase consists of hardcore boson pairs and it is, in principle, possible to map the system to an effective SSH model for the spinless fermions and study the topological features in the context of the Rice-Mele model [54–56].

ACKNOWLEDGMENTS

The computational simulations were carried out using the Param-Ishan HPC facility at the Indian Institute of Technology – Guwahati, India. S.G. acknowledges support by the Swiss National Science Foundation under Division II. T.M. acknowledges DST-SERB for the early career grant through Project No. ECR/2017/001069.

[1] M. Greiner, O. Mandel, T. Esslinger, T. W. Hänsch, and I. Bloch, Nature (London) **415**, 39 (2002).

[2] D. Jaksch, C. Bruder, J. I. Cirac, C. W. Gardiner, and P. Zoller, Phys. Rev. Lett. **81**, 3108 (1998).

[3] M. Lewenstein, A. Sanpera, and V. Ahufinger, Contemp. Phys. **54** (2013).

[4] I. B. Spielman, W. D. Phillips, and J. V. Porto, Phys. Rev. Lett. **98**, 080404 (2007).

[5] D. van Oosten, P. van der Straten, and H. T. C. Stoof, Phys. Rev. A **63**, 053601 (2001).

[6] I. Danshita, J. E. Williams, C. A. R. Sá de Melo, and C. W. Clark, Phys. Rev. A **76**, 043606 (2007).

[7] G. Vidal, Phys. Rev. Lett. **93**, 040502 (2004).

[8] J. Sebby-Strabley, M. Anderlini, P. S. Jessen, and J. V. Porto, Phys. Rev. A **73**, 033605 (2006).

[9] J. Sebby-Strabley, B. L. Brown, M. Anderlini, P. J. Lee, W. D. Phillips, J. V. Porto, and P. R. Johnson, Phys. Rev. Lett. **98**, 200405 (2007).

[10] G. J. Cruz, R. Franco, and J. Silva-Valencia, J. Phys.: Conf. Ser. **687**, 012065 (2016).

[11] M. Anderlini, J. Lee Patricia, L. Brown Benjamin, J. Sebby-Strabley, D. Phillips William, and J. V. Porto, Nature (London) **448**, 452 (2007).

[12] W. P. Su, J. R. Schrieffer, and A. J. Heeger, Phys. Rev. Lett. **42**, 1698 (1979).

[13] S. Ryu and Y. Hatsugai, Phys. Rev. Lett. **89**, 077002 (2002).

[14] J. Zak, Phys. Rev. Lett. **62**, 2747 (1989).

[15] P. Delplace, D. Ullmo, and G. Montambaux, Phys. Rev. B **84**, 195452 (2011).

[16] L.-J. Lang, X. Cai, and S. Chen, Phys. Rev. Lett. **108**, 220401 (2012).

[17] S. R. Manmana, A. M. Essin, R. M. Noack, and V. Gurarie, Phys. Rev. B **86**, 205119 (2012).

[18] T. Yoshida, R. Peters, S. Fujimoto, and N. Kawakami, Phys. Rev. Lett. **112**, 196404 (2014).

[19] F. Grusdt, M. Höning, and M. Fleischhauer, Phys. Rev. Lett. **110**, 260405 (2013).

[20] M. Atala, M. Aidelsburger, J. T. Barreiro, D. Abanin, T. Kitagawa, E. Demler, and I. Bloch, Nat. Phys. **9**, 795 (2013).

[21] C. Schweizer, M. Lohse, R. Citro, and I. Bloch, Phys. Rev. Lett. **117**, 170405 (2016).

[22] M. Lohse, C. Schweizer, O. Zilberberg, M. Aidelsburger, and I. Bloch, Nat. Phys. **12**, 350 (2016).

[23] S. Nakajima, T. Tomita, S. Taie, T. Ichinose, H. Ozawa, L. Wang, M. Troyer, and Y. Takahashi, Nat. Phys. **12**, 296 (2016).

[24] S. de Léséleuc, V. Lienhard, P. Scholl, D. Barredo, S. Weber, N. Lang, H. P. Büchler, T. Lahaye, and A. Browaeys, arXiv:1810.13286.

[25] S. Will, T. Best, U. Schneider, L. Hackermüller, D.-S. Lühmann, and I. Bloch, Nature (London) **465**, 197 (2010).

[26] D. S. Petrov, Phys. Rev. Lett. **112**, 103201 (2014).

[27] D. S. Petrov, Phys. Rev. A **90**, 021601(R) (2014).

[28] P. R. Johnson, E. Tiesinga, J. V. Porto, and C. J. Williams, New J. Phys. **11**, 093022 (2009).

[29] A. J. Daley, J. M. Taylor, S. Diehl, M. Baranov, and P. Zoller, Phys. Rev. Lett. **102**, 040402 (2009).

[30] A. Safavi-Naini, J. von Stecher, B. Capogrosso-Sansone, and S. T. Rittenhouse, Phys. Rev. Lett. **109**, 135302 (2012).

[31] L. Bonnes and S. Wessel, Phys. Rev. Lett. **106**, 185302 (2011).

[32] B. Chen, X. Huang, S. Kou, and Y. Zhang, Phys. Rev. A **78**, 043603 (2008).

[33] T. Sowiński, R. W. Chhajlany, O. Dutta, L. Tagliacozzo, and M. Lewenstein, Phys. Rev. A **92**, 043615 (2015).

[34] M. Singh, T. Mishra, R. V. Pai, and B. P. Das, Phys. Rev. A **90**, 013625 (2014).

[35] M. Singh, S. Mondal, B. K. Sahoo, and T. Mishra, Phys. Rev. A **96**, 053604 (2017).

[36] S. Greschner, L. Santos, and T. Vekua, Phys. Rev. A **87**, 033609 (2013).

[37] A. F. Hincapie-F, R. Franco, and J. Silva-Valencia, Phys. Rev. A **94**, 033623 (2016).

[38] C. Avila, R. Franco, A. Souza, M. Figueira, and J. Silva-Valencia, Phys. Lett. A **378**, 3233 (2014).

[39] J. Silva-Valencia and A. Souza, Eur. Phys. J. B **85**, 161 (2012).

[40] T. Giamarchi, *Quantum Physics in One Dimension* (Clarendon, Oxford, UK, 2003), Vol. 121.

[41] M. Di Liberto, A. Recati, I. Carusotto, and C. Menotti, Phys. Rev. A **94**, 062704 (2016).

[42] M. Di Liberto, A. Recati, I. Carusotto, and C. Menotti, Eur. Phys. J.: Spec. Top. **226**, 2751 (2017).

[43] M. Singh, A. Dhar, T. Mishra, R. V. Pai, and B. P. Das, Phys. Rev. A **85**, 051604(R) (2012).

[44] S.-J. Gu, Int. J. Mod. Phys. B **24**, 4371 (2010).

[45] A. Dhar, M. Maji, T. Mishra, R. V. Pai, S. Mukerjee, and A. Paramekanti, Phys. Rev. A **85**, 041602(R) (2012).

[46] D. Muth, A. Mering, and M. Fleischhauer, Phys. Rev. A **77**, 043618 (2008).

[47] W. S. Bakr, J. I. Gillen, A. Peng, S. Fölling, and M. Greiner, Nature (London) **462**, 74 (2009).

[48] J. F. Sherson, C. Weitenberg, M. Endres, M. Cheneau, I. Bloch, and S. Kuhr, Nature (London) **467**, 68 (2010).

[49] D. González-Cuadra, P. R. Grzybowski, A. Dauphin, and M. Lewenstein, Phys. Rev. Lett. **121**, 090402 (2018).

[50] D. González-Cuadra, A. Dauphin, P. R. Grzybowski, P. Wójcik, M. Lewenstein, and A. Bermudez, Phys. Rev. B **99**, 045139 (2019).

[51] T. Yoshida, I. Danshita, R. Peters, and N. Kawakami, Phys. Rev. Lett. **121**, 025301 (2018).

[52] Y. E. Kraus, Y. Lahini, Z. Ringel, M. Verbin, and O. Zilberberg, Phys. Rev. Lett. **109**, 106402 (2012).

[53] M. Nakagawa, T. Yoshida, R. Peters, and N. Kawakami, Phys. Rev. B **98**, 115147 (2018).

[54] M. J. Rice and E. J. Mele, Phys. Rev. Lett. **49**, 1455 (1982).

[55] A. Hayward, C. Schweizer, M. Lohse, M. Aidelsburger, and F. Heidrich-Meisner, Phys. Rev. B **98**, 245148 (2018).

[56] S. Greschner, S. Mondal, and T. Mishra (unpublished).